

CONF-9609140-76

Atomic Collisions with 33-TeV Lead Ions

C. R. Vane, S. Datz, H. F. Krause, P. F. Dittner, and E. F. Deveney

*Physics Division, Oak Ridge National Laboratory
Oak Ridge, Tennessee 37831-6377 USA*

H. Knudsen

*Institute of Physics, Aarhus University
DK-8000, Aarhus C, Denmark*

Per Grafström

CERN, CH-1211, Geneva 23, Switzerland

R. Schuch and H. Gao

*Manne Siegbahn Laboratory at Stockholm University
Frescativägen 24, S-104 05, Stockholm, Sweden*

R. Hutton

*Atomic Spectroscopy, University of Lund
Sölvegatan 14, S-223 62, Lund Sweden*

RECEIVED
OCT 10 1996
OSTI

ABSTRACT

Recent availability of relativistic and ultrarelativistic beams of heavy ions has permitted the first controlled studies of atomic collisions at energies sufficient to measure effects of several new basic phenomena. These include measurements substantiating recently predicted finite nuclear size effects resulting in a reduction in the total electronic energy loss of heavy ions in matter, and measurements of Coulomb collisions in which electrons are excited from the Dirac negative energy continuum. Measurements of total energy loss, free electron-positron pair production, and electron capture from pair production have been recently performed using 33-TeV Pb^{82+} ions from the CERN SPS accelerator in Geneva. Results of these studies are presented, along with comparisons with relevant theory.

DISCLAIMER

This report was prepared as an account of work sponsored by an agency of the United States Government. Neither the United States Government nor any agency thereof, nor any of their employees, makes any warranty, express or implied, or assumes any legal liability or responsibility for the accuracy, completeness, or usefulness of any information, apparatus, product, or process disclosed, or represents that its use would not infringe privately owned rights. Reference herein to any specific commercial product, process, or service by trade name, trademark, manufacturer, or otherwise does not necessarily constitute or imply its endorsement, recommendation, or favoring by the United States Government or any agency thereof. The views and opinions of authors expressed herein do not necessarily state or reflect those of the United States Government or any agency thereof.

The submitted manuscript has been authored by a contractor of the U.S. Government under Contract No. DE-AC0596OR22464. Accordingly, the U.S. Government retains a nonexclusive, royalty-free license to publish or reproduce the published form of this contribution, or allow others to do so, for U.S. Government purposes.

MASTER

DISCLAIMER

Portions of this document may be illegible in electronic image products. Images are produced from the best available original document.

I. Introduction

At ultrarelativistic energies, peripheral collisions between heavy, highly charged atoms produce extremely intense, rapidly varying electromagnetic fields give rise to very large ionization cross sections, diminished electron capture cross sections, and copious lepton-pair formation. These collisions are fundamentally different from those involving singly charged projectiles because the coupling constant, $Z\alpha$, can be large (≥ 0.5) in heavy systems. Lepton-pair production in these systems is especially interesting because the collision strength can be varied continuously, from regions of low charge and energy, where past applications of low-order perturbative methods are suitable, to higher energy and charge regimes where first-order perturbative calculations are known to occasionally give unphysical results. Recent progress toward realization of energetic ion-ion colliders such as the Relativistic Heavy-Ion Collider (RHIC) at Brookhaven National Laboratory and the Large Hadron Collider (LHC) at CERN has sparked renewed interest in electromagnetic phenomena at very high energies.

Figure 2 shows predicted cross sections [1] for one-electron ionization and capture by lead ions in gold. As shown there, ionization of $Pb^{81+}(1s)$ continues to increase as the beam energy $(\gamma - 1)M_{Pb}c^2$ increases $\left(\gamma = 1/\sqrt{1 - \beta^2}, \beta = v/c\right)$. Radiative and non-radiative electron capture (REC and NRC) fall dramatically. Electron capture from pair production (σ_{vac}) increases logarithmically with energy, dominating other mechanisms above ~ 10 GeV/nucleon ($\gamma \sim 10$). At sufficiently high energies, the electron deBroglie wavelength becomes comparable to nuclear radii and nuclear size effects are predicted [2] to become important in limiting direct Knock-On electron energies and substantially reducing total energy loss. Other electromagnetic nuclear excitation processes also grow logarithmically with energy, and together with electron capture from pair production

become important as the limiting loss mechanisms for operation of relativistic heavy-ion storage rings (colliders).

We have measured production of positrons from electron-positron pairs for 33-TeV Pb ions from the CERN SPS accelerator facility to determine differential cross sections ($d\sigma/dp+$) and set limits on contributions from multiple-pair formation in single collisions. We have also measured electron capture and loss, as well as, total energy loss in much thicker targets. Results of these recent studies and comparisons with theory are presented below.

II. Free pair production

Electron and positrons produced in thin targets of carbon ($(CH_2)_x$), Al, Pb, and Au were separated and dispersed in a uniform-field magnetic spectrograph as shown in Fig.2. With minor modifications, the experimental setup has been described in much greater detail in [4]. Positrons with momenta 1–12 MeV/c were bent through $\sim 180^\circ$ and directed onto an array of 81 circular (2 cm diameter) silicon surface-barrier detectors (depletion depth 300 μm). The detectors were arranged in five horizontal rows, covering 52% of the available area as shown in Fig. 2. Signals from each detector were independently processed.

Projectile ions passing through the very thin ($\leq 10 \text{ mg/cm}^2$) targets were mainly unaffected. The primary ions continued downstream where they were used in a large scale nuclear experiment designated WA98 searching for signatures of quark-gluon plasma formation. Signals from WA98 fast scintillator beam counters and from a Zero Degree Calorimeter (ZDC) were used to identify, count, and provide timing for full-energy lead ions detected in coincidence with positrons from our targets.

In our previous measurements with 6.4-TeV sulfur ions [4], both the electron and positron constituting a pair were measured using two arrays of detectors located on opposite sides of the target. Attempts to measure pair electrons were abandoned in the currently reported measurements because extrapolation of the sulfur data and,

independently, calculations based on relativistic Born approximation differential cross sections for binary ion-electron collisions, both predict high probabilities for simultaneous emission of a direct Knock-On (KO) electron from the targets for every pair-producing collision.

Positrons were detected as single-hits, i.e., one count on any of 81 detectors, or as higher multiplicity hits ($M > 1$), if more than one detector triggered with a 100 nsec coincidence window. Yields of single-positrons were converted to differential cross sections. Momentum distributions for all targets were observed to be the same within statistical error. In Fig. 3, we compare single-positron ($d\sigma/dp+$) for 33-TeV Pb ions on Au, with data taken previously for 6.4-TeV S ions. We note similarity in the two distributions, but with some indication of an increase in cross section above ~ 8 MeV/c for Pb ions. Lowest order QED calculations predict identical distributions.

We note that previous S ion measurements of coincident electrons and positrons showed that the particles shared the pair energy in a very uncorrelated way, contrary to some theoretical results indicating substantial correlation among components of multiple-pairs. We have assumed that positron momenta were completely uncorrelated in the analysis for multiple-pair effects that follows.

Multiple-pair contributions to total pair production were investigated by two methods. In the first, the total yields of positrons, counted as single hits on the detector array were measured in precisely the same way for targets of $(CH_2)_x$, Al, Pd, and Au. The overall probability of detecting any emitted positron was low ($\sim 10\%$), so that, if the individual positrons were uncorrelated in momenta, single-hit additions to the total yield from double-pairs would occur at approximately twice the rate of double-pair production. Triple-pairs would add at ~ 3 times the triple-pairs rate, etc.

Single-pair yields scale very nearly as the product of the squares of the charges of the colliding atoms (see Fig. 3). However, multiple pairs yields should scale approximately as $\sim Z_T^{2M}$, where M is the pair multiplicity, i.e., $M=2$ for double pairs. Theoretical calculations of the strength of multiple pair production vary, but generally predict $\sim 2-5\%$ $M=2$ pairs compared to single pairs, falling binomially to $\sim 0.2-0.2\%$ for three pairs. A substantial contribution from multiple pairs to single-hit positron yields should then be manifested as a deviation from strict Z_T^2 scaling. Figure 4 shows the results of fitting measured single-positron yields to $\sim Z_T^P$, $P = 2.03 \pm 0.03$. The curve marked "Theory" displays results based on multiple pair cross-section calculations by Guclu et al. [5], and assuming uncorrelated momentum independence of all the ejected positrons. The curve marked "Theory x4" indicates the effect of increasing the multiple-pairs (higher-order Z_T^P terms) component by x4 over the theoretical value. Our results agree with the predictions [5], but include the possibility of no multiple pairs.

The second method for investigating multiple pairs was more direct. Data were collected for events in which more than one positron detector triggered a count within 100 nsec. Multiple counts of M -positrons within the time window occurred for real positrons from multiple pairs generated in a single collision, from accidental coincidences of multiple collisions, and from electronic cross-talk among detectors and electronics. The measured ratios of yields of double counts to single counts, $R(M=2/M=1)$, corrected for constant cross-talk are displayed in Fig. 5 as a function of Z_T . The experimental results support very low multiple pair production of $R = 0.025 \pm 0.027$ for gold.

III. Energy Loss

The stopping of high energy ions in matter is primarily determined by collisions with electrons and resulting transfers of energy from the moving ion to the target. At sufficiently high energies the deBroglie wavelength of the electron in the frame of the

projectile becomes the same order as the size of the heavy ion charge distribution, i.e., the nuclear radius. Lindhard and Sorensen (LS) [Ref. 2] have recently shown that such effects can lead to a significant reduction in electronic stopping power for heavy relativistic ions. The energy loss of a fully-stripped ion Z_p , velocity v , penetrating a thickness Δx of electron density n_e can be expressed in terms of a nearly constant parameter L , such that

$$\Delta E = \Delta x \left[\frac{4\pi Z_p^2 e^4}{m_0 v^2} \right] n_e L$$

where m_0 is the electron rest mass. At relativistic energies L can be written in terms of the plasmon frequency of the target medium ω_p and a second parameter ΔL as

$$L = \ell n \left[\frac{2\gamma m_0 c^2}{\hbar \omega_p} \right] - 1/2 + \Delta L.$$

In the *LS* formulation ΔL contains a number of relatively small correction terms, including the effect of an extended charge on the scattering of high energy electrons. At $\gamma = 168$, target electrons in the projectile frame have energies of 86 MeV and a deBroglie wavelength of ~ 2 Fermi - or about 1/3 of the Pb nuclear radius.

To measure precise energy changes at such high energies, we used the experimental setup indicated schematically in Fig. 6, which is primarily composed of an existing transport beam line H3 at the CERN SPS West experimental hall. A target manipulator was installed at the output of the TAX collimator assembly, located just after beam extraction from the SPS ring.

Lead particles passing through the target were vertically deflected and magnetically dispersed by dipole steering magnets. A vertical y -collimator assembly was located at the point of maximum rigidity dispersion ~ 150 m downstream of the target. This 1-m-long iron collimator was scanned across the main beam (or a chosen product ion) in 2 mm steps to produce a transmission profile of ions selected for transport down the rest of the beam

line to the ZDC. Momentum calibration was obtained both from field calculations and from the peak positions of ^{208}Pb and ^{207}Pb (formed by neutron loss in windows and air) or ^{207}Tl (formed by proton loss). The measured energy resolution is $<1 \times 10^{-3}$, permitting peak position determination to a precision of 1×10^{-4} . Measurements were performed for targets of C, Si, Cu, Sn, and Pb in thicknesses giving energy losses of 0.1%, 0.2%, 0.4%, and 0.8% of the total energy. Experimental values of L extracted from the measured energy losses and thicknesses are shown in Fig. 7, along with results of calculations by Lindhard and Sorensen [2] for point and extended Pb nuclei which differ by $\sim 15\%$. The error in the measured L values is 0.5-1.0%. Our measurements confirm the predicted nuclear size effect in reducing stopping, but there appears to be an unexplained systematic deviation of experiment and theory for heavy targets.

IV. Electron Capture and Loss

As shown in Fig.1, at very high energies electron capture is expected to proceed mainly by an entirely new phenomena. Electrons initially occupying states in the Dirac negative energy continuum can be promoted into vacant bound states (1s,2s,2p,...) of the Pb^{82+} . The process is termed electron capture from pair production or vacuum capture. There is firm theoretical basis for expecting reliable extrapolation from measurements made at $\gamma > 100$, to the much higher energies needed for colliders ($\gamma = 2 \times 10^5$ for RHIC and 2×10^7 for LHC). This applies because the vacuum capture cross section must behave asymptotically (above $\gamma > 100$) as $\sim A \ln \gamma + B$, where A and B are constants [6].

To measure the vacuum capture cross section, we have used the H3 beam line as a charge-state analyzer, and measured the fractions $\text{Pb}^{81+}/\text{Pb}^{82+}$ of one-electron ions produced and surviving as a function of target thickness and atomic number Z_T . The method used was identical to that described previously for energy loss measurements, except that Pb^{81+} and Pb^{82+} yields were obtained as background-corrected integrals of

scanned beam profiles for targets of C, Al, Cu, and Au. An example set of data for Au targets is shown in Fig.8. With no target in place, the fraction of Pb^{81+} was found to be $\sim 1.5 \times 10^{-3}$. As targets were inserted the fraction decreased to a near constant equilibrium value $\sim 0.8 \times 10^{-3}$ for Au. The excess of one-electron ions in the incident beam arises from interaction of the beam with air and Al beamline entrance windows located upstream of our targets, yet downstream of any bending magnets. Interestingly, low- Z_T targets lead to enhanced Pb^{81+} fractions, so that the upstream air gaps produced significantly higher yields of one-electron ions than equilibrium thicknesses of heavy targets. The curve shown in Fig. 8 is the result of a fit to a two-component (Pb^{81+} and Pb^{82+}) model from which electron capture and loss cross sections can be extracted. Within this model, $f(x)$ – the fraction of Pb^{81+} after target thickness x – is given by

$$f(x) = f_{equil} + (f_0 - f_{equil}) \exp[-(\sigma_{cap} + \sigma_{loss})x],$$

where f_{equil} and f_0 are the equilibrium and incident fractions of Pb^{81+} , respectively, and σ_{cap} and σ_{loss} are the total effective electron capture and loss cross sections. By definition $f_{equil} = \sigma_{cap} / \sigma_{loss}$. Results of fits to the data are given in Table I where they are compared with calculations by Anholt and Becker [1]. We obtain, after correction for small contributions from REC, cross sections for electron capture from pair production (Vacuum Capture) of 73b for $Pb^{82+} + Au$ and 1.4 b for $Pb^{82+} + Al$. Estimated total errors are $\pm 25\%$ in each case. The Au cross section is larger than the best theoretical prediction which is ~ 50 b for 1s capture [7], and may include some fraction due to capture to excited states ($n \geq 2$) which survive collisional ionization in the same target. The predicted Au ionization cross section for $Pb^{81+}(1s)$ is 61 kb [1]. However, there is an additional contribution to electron loss through primary excitation followed by ionization of the excited state in a second collision. This can occur only because the lifetimes of excited states are Lorentz extended by a factor of $\gamma = 168$. In high- Z_T targets where ionization of

excited states is very rapid, excitation followed by secondary ionization competes with radiative decay stabilization, and provides a significant portion of the total loss process. In low- Z_T targets ($Z_T < 20$) radiation proceeds much more quickly than the $\sim Z_T^2$ reduced ionization cross sections. The measured f_{equil} are plotted in Fig. 9 as a function of Z_T , and compared with expected values obtained from [1]. We observed for C targets $f_{equil} = 1.8 \times 10^{-3}$, significantly enhanced above values for heavier targets. This effect can explain our observation of the excess (1.5×10^{-3}) of one-electron Pb ions incident on our targets as due to equilibrium in N_2 (air) (1.6×10^{-3} – see Fig. 9), followed by partial stripping in a thin Al window located just upstream of our target. We note that this effect would become especially obvious in heavy gas targets, where transit time between collisions would permit radiative stabilization and lead to lower effective total loss cross sections, i.e., higher f_{equil} values.

We plan to soon (fall 1996) re-measure the capture and loss cross sections with an improved technique in which the incident beam is cleaned of contaminant charge states using the first bending magnets shown in Fig. 6 as a beam purifier and the second magnets as an analyzer. This will allow us to make much more accurate measurements of the growth of Pb^{81+} with increasing target thicknesses, and of the capture cross sections. Gas target measurements are planned for 1997.

Acknowledgements

Research sponsored by the U.S. Department of Energy, Office of Basic Energy Sciences, Division of Chemical Sciences, under Contract No. DE-AC05-96OR22462 with Lockheed Martin Energy Research Corporation.

References

1. R. Anholt and U. Becker, *Phys. Rev. A* **36**, 4628 (1987).
2. J. Lindhard and A. Sorensen, *Phys. Rev. A* **53**, 2443 (1996).
3. A. Belkacem, H. Gould, B. Feinberg, R. Bossingham, and W. E. Meyerhof, *Phys. Rev. Lett.* **71**, 1514 (1993); *Phys. Rev. Lett.* **73**, 2432 (1994).
4. C. R. Vane, S. Datz, P. F. Dittner, H. F. Krause, R. Schuch, H. Gao, and R. Hutton, *Phys. Rev. A* **50**, 2313 (1994).
5. M. C. Guclu, J. C. Wells, A. S. Umar, M. R. Strayer, and D. J. Ernst, *Phys. Rev. A* **51**, 1836 (1995).
6. A. Baltz, M. Rhoades-Brown, and J. Weneser, *Phys. Rev. A* **47**, 3444 (1993).
7. The 50 b capture cross section was calculated by M. Strayer and J. Wells (unpublished) using the method described by A. Baltz, M. Rhoades-Brown, and J. Weneser, *Phys. Rev. A* **44**, 5569 (1991).

Figure Captions

- Fig. 1. Calculated cross sections (see Ref. 1) for Pb ions at relativistic energies $KE = (\gamma-1)M_p C^2$. Ionization (σ_{ioniz}) is for $\text{Pb}^{81+}(1s) + \text{Au}$. Non-radiative electron capture (σ_{NRC}) contributes only a small fraction of total capture at all energies within the approximations made in these calculations. Capture from pair production (σ_{vac}) dominates above $\gamma \approx 10$.
- Fig. 2. Schematic diagram of uniform field positron spectrometer showing (a) 81 detector array and (b) example trajectories for positrons and electrons emitted from the target.
- Fig. 3. Measured singly-differential cross sections for positrons formed in Coulomb collisions of 33-TeV lead ions with a gold target. Previous results for 6.4-TeV sulfur ions on gold are indicated by the dashed curve. For comparison, the sulfur data have been scaled by the square of projectile nuclear charges Z_p , i.e., $(82/16)^2$ and as $(\ell n \gamma)^3$, as predicted by equivalent photon approximation calculations. A power-law fit of the measured integrated positron yields versus projectile Z_p gives $\sim (Z_p^{2.0 \pm 0.1})$.
- Fig. 4. Integrated yields (1–12 MeV/c) of single-positrons measured as a function of target nuclear charge Z_T , for carbon (polypropylene), aluminum, palladium, and gold. The solid curves display as indicated, fits to experimental data, yields calculated from theoretical cross sections from Ref. 5 (theory), and the effect of increasing multiple pairs contributions by a factor of 4 (Theory X4).
- Fig. 5. Measured ratios of yields of positron detector double-hits to single-hits plotted versus target Z_T . Solid curve displays calculated ratios assuming the theoretical cross sections for single- and multiple-pairs from Ref. 5. Dashed curve shows the effect of increasing the multiple-pairs relative yields by a factor of 4.

- Fig. 6. Schematic diagram of the WA99 charge-changing and energy-loss apparatus which uses magnetic components of beam line H3 at the SPS West Hall and the WA98 ZDC together as a high-resolution magnetic analyzer. Beam profiles were measured for remotely positioned targets by scanning a narrow (2 mm) collimator across the selected product ions in the plane of magnetic dispersion
- Fig. 7. Measured and calculated values of L for 33-TeV Pb ions as a function of target material, Z_T .
- Fig. 8. One-electron Pb^{81+} fractions measured as a function of Au target thickness. The solid curve displays results of a two-component fit and gives a total capture cross section (σ_{cap}) of 75 barns and a total electron loss cross section (σ_{loss}) of 81 k barns.
- Fig. 9. Measured Pb^{81+} equilibrium fractions for C, Al, Cu, and Au targets. The solid curves display a fit to the data and results expected from cross sections calculated by R. Anholt and U. Becker (Ref. 1).

Table I. Measured and calculated cross sections for ionization and capture by 33-TeV Pb ions.

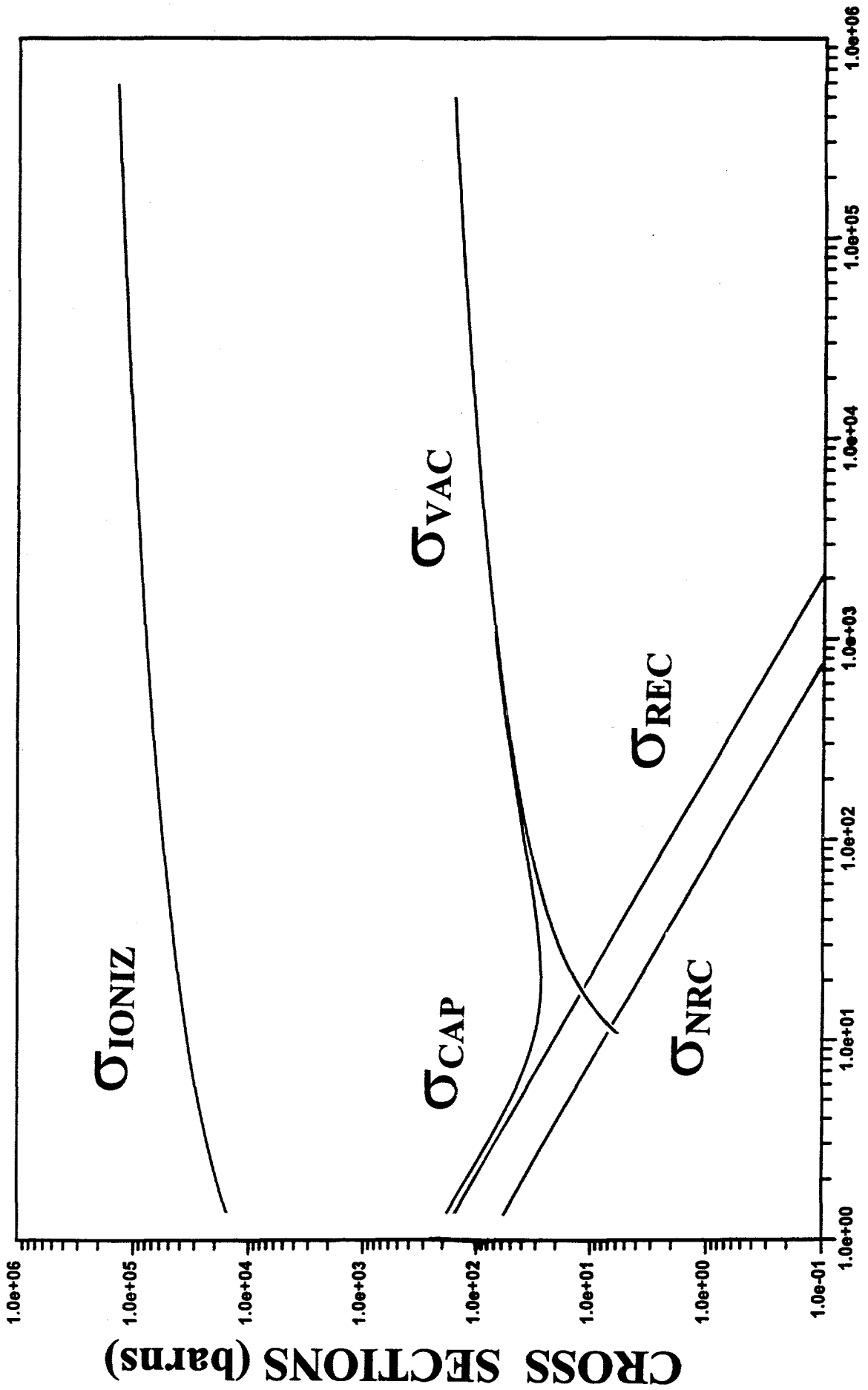
| Z_T | f_{EQUIL} | LOSS | TOTAL CAPTURE | REC + NRC | VACUUM CAPTURE |
|-------|-----------------------|--------------|-----------------|-----------|----------------|
| 6 | 1.80×10^{-3} | ----- / 490* | ----- / (0.9)** | 0.1 | 0.8 / 0.3# |
| 13 | 1.14×10^{-3} | 1370 / 2042 | 1.6 / (2.4) | 0.2 | 1.4 / 1.4 |
| 29 | 8.40×10^{-4} | ----- / 13 k | ----- / (9.5) | 0.5 | 9.0 / 6.7 |
| 79 | 9.25×10^{-4} | 81 k / 94 k | 75 / (87) | 1.7 | 73 / 50 |

* R. Anholt and U. Becker, *Phys. Rev. A* **36**, 4628 (1987). Cross sections for 1s ionization corrected for secondary 1s-2p excitation and ionization competing with radiative decay.

** Capture cross sections calculated from measured equilibrium 81+ charge state fractions and theoretical loss cross sections.

Theoretical vacuum capture cross section from Ref. 1.

Pb 82+ + Au



γ FIXED TARGET

Figure 1

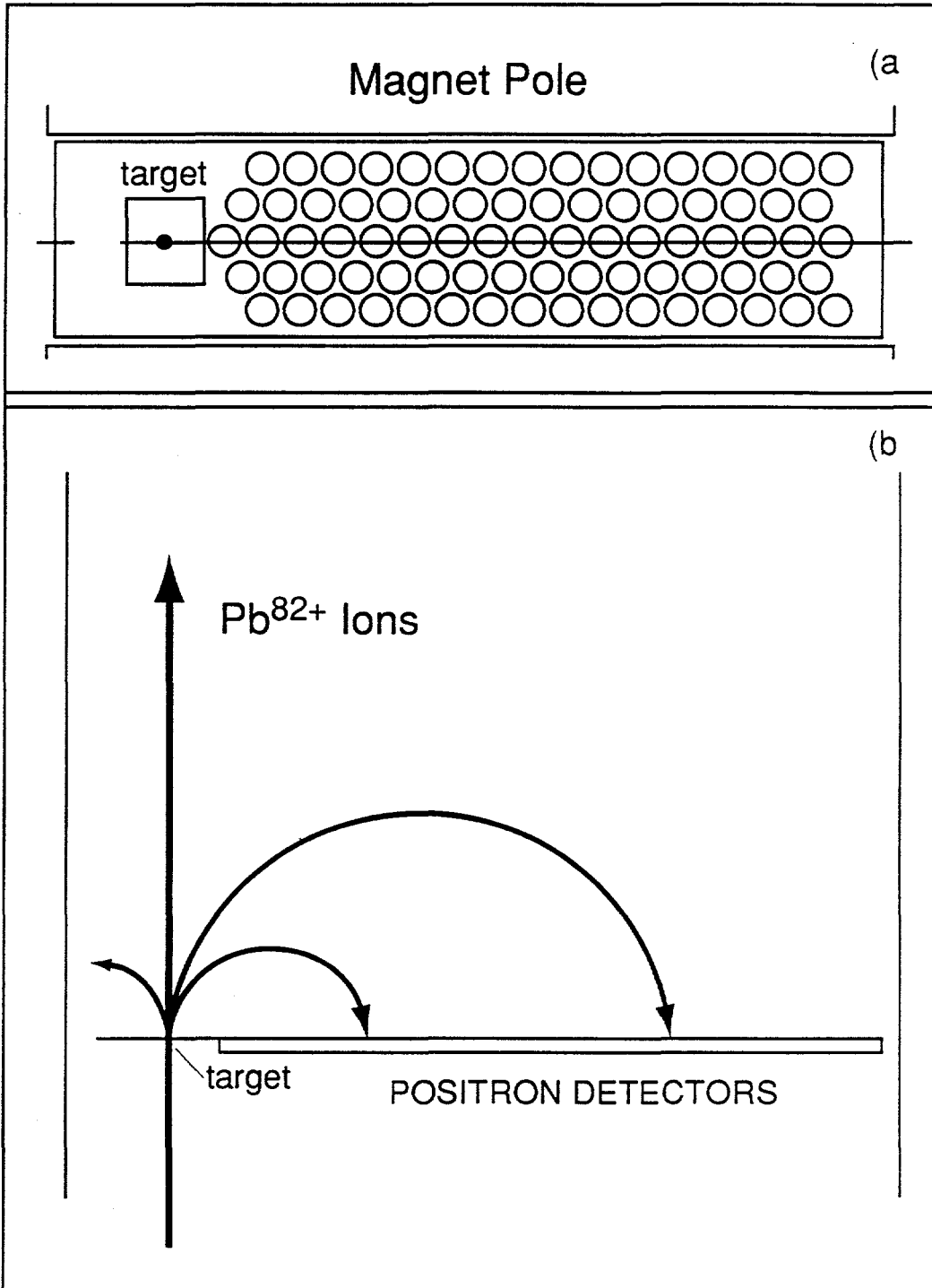


Figure 2

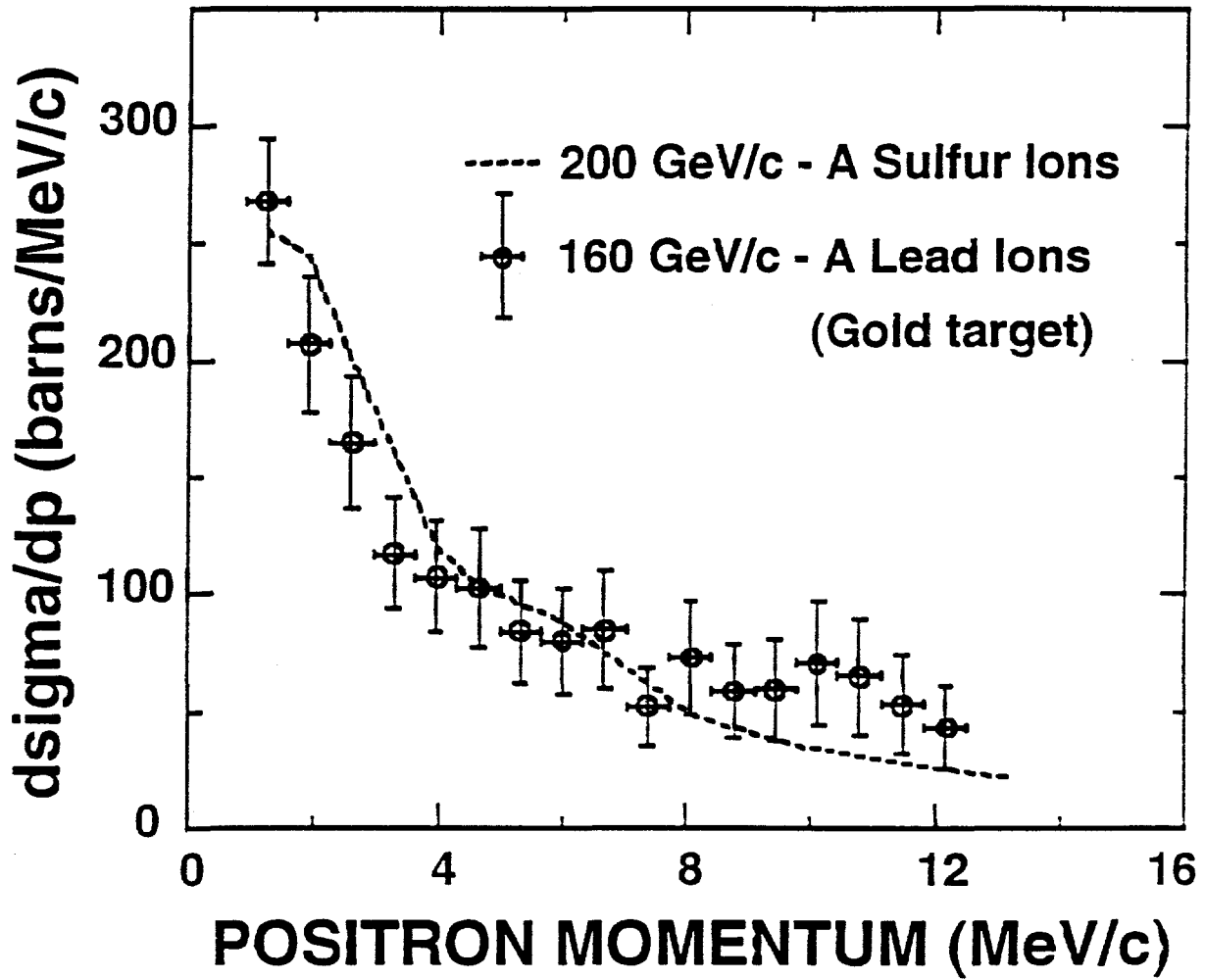


Figure 3

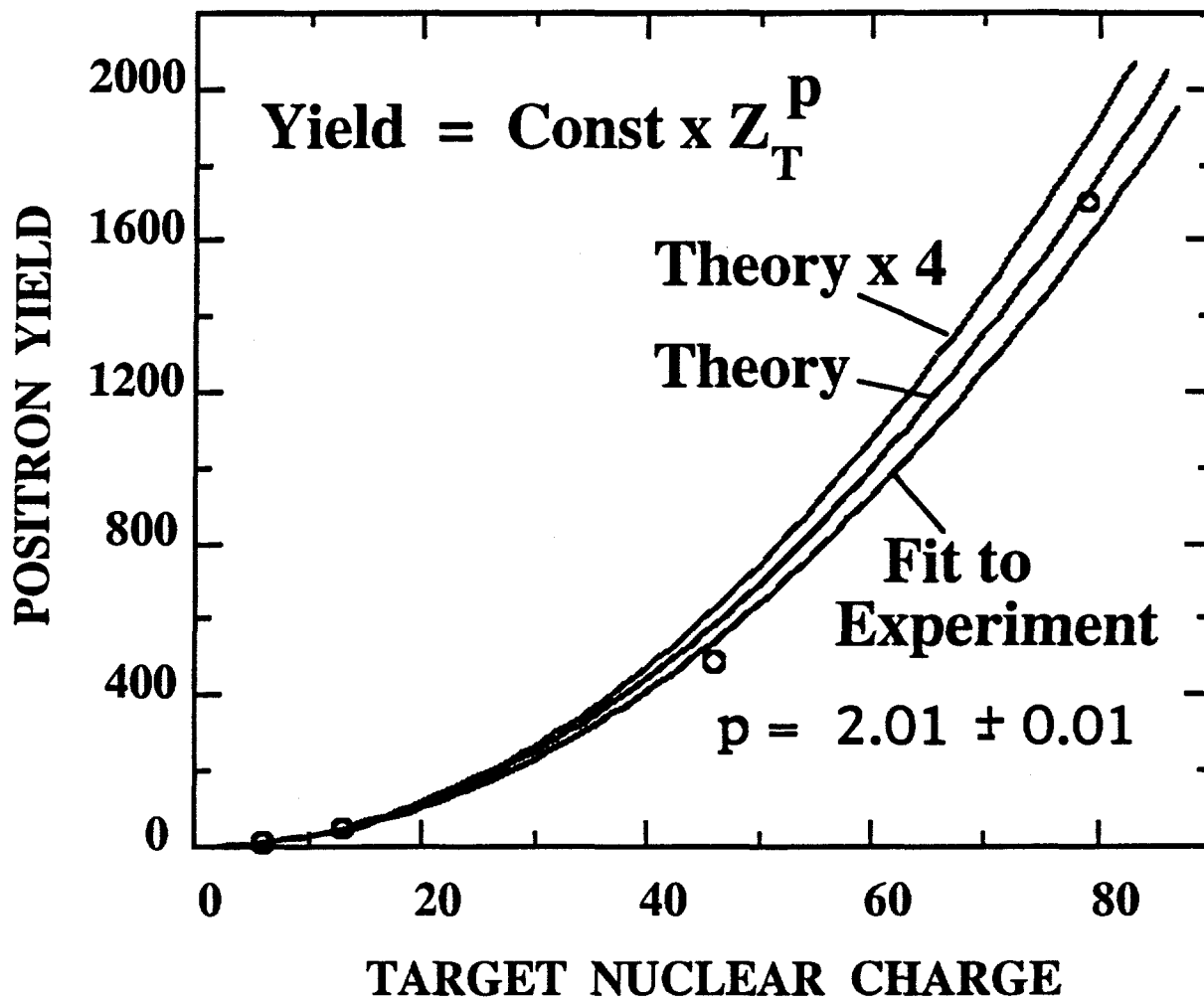


Figure 4

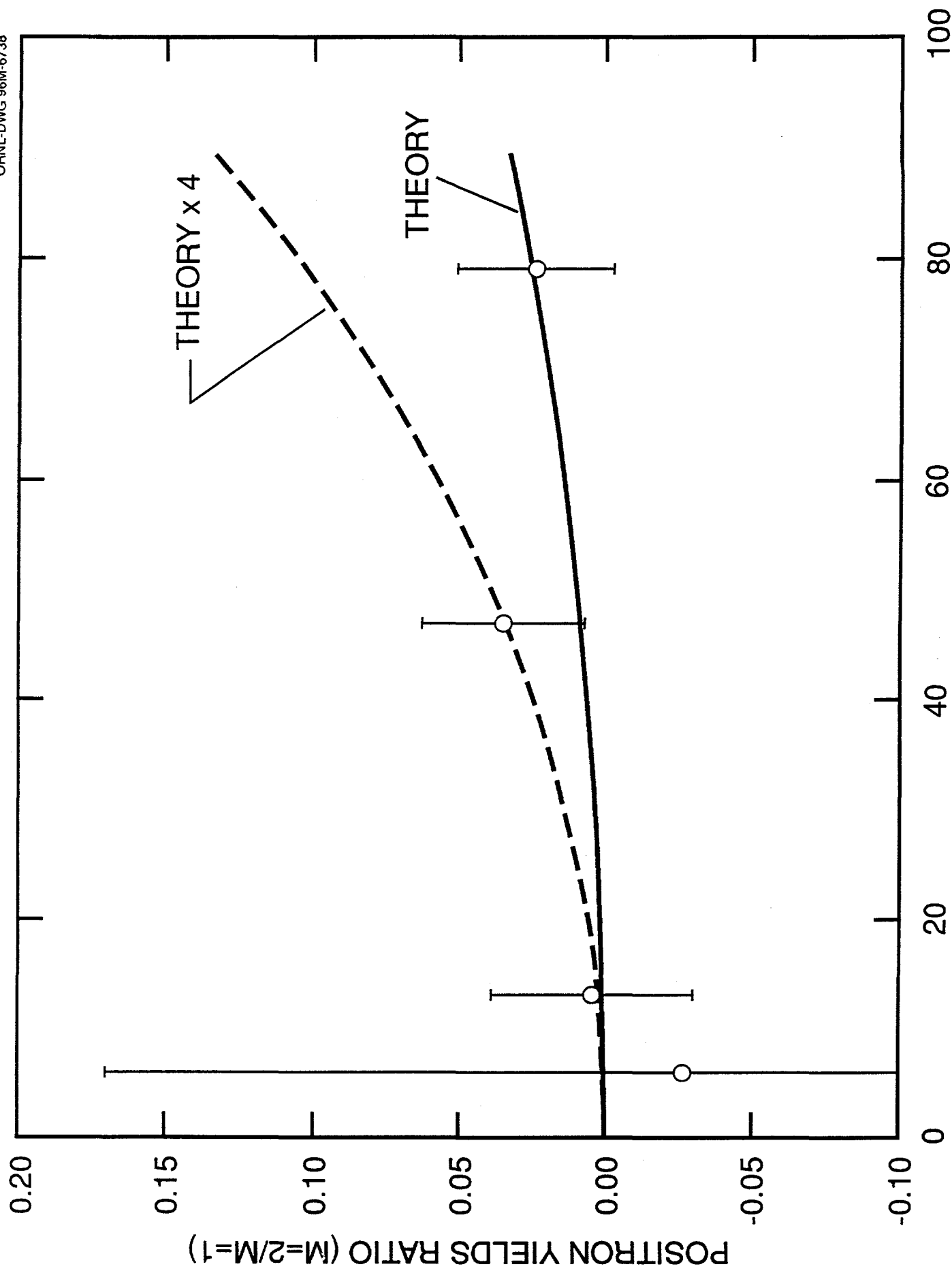


Figure 5

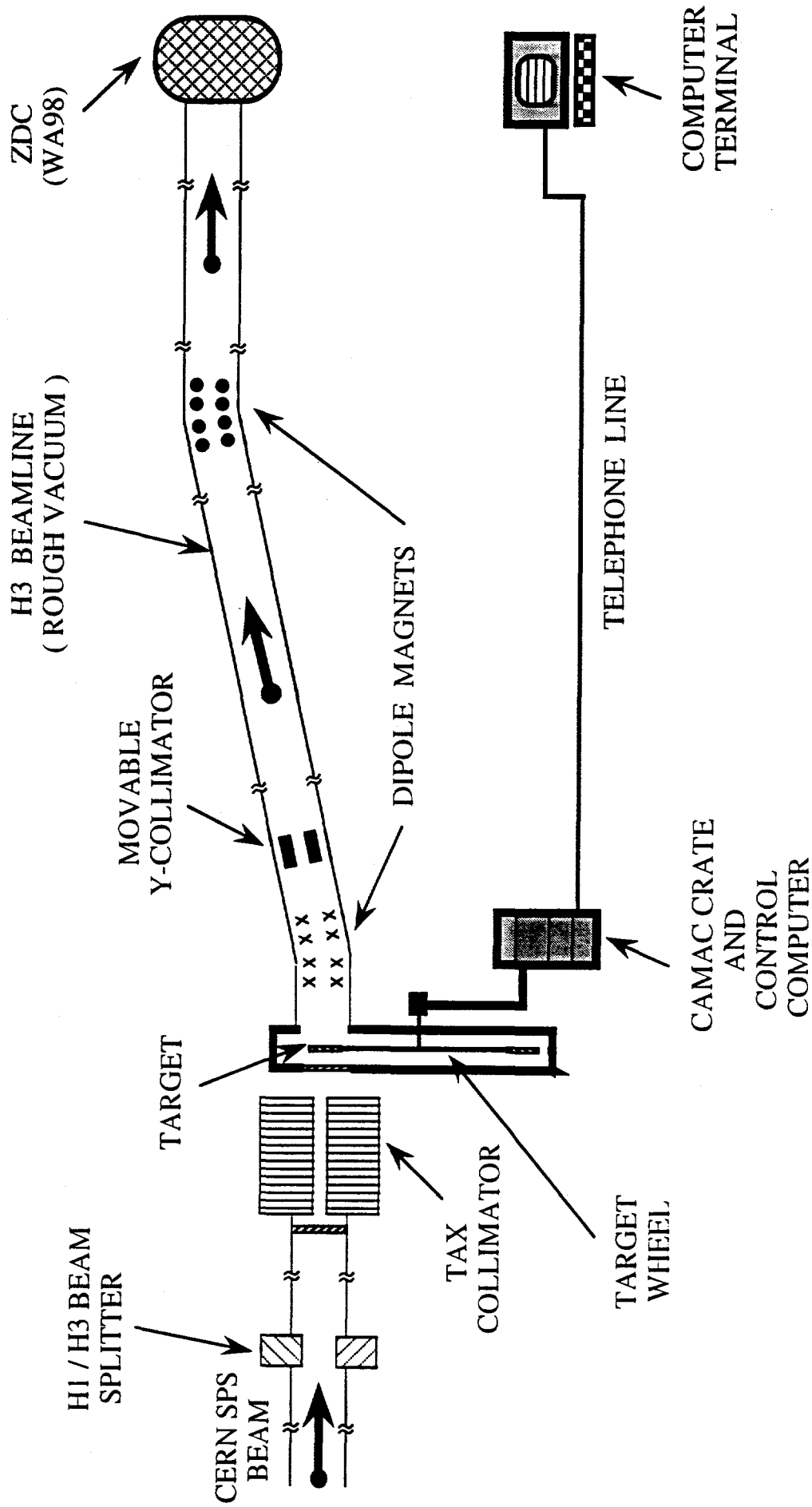


Figure 6

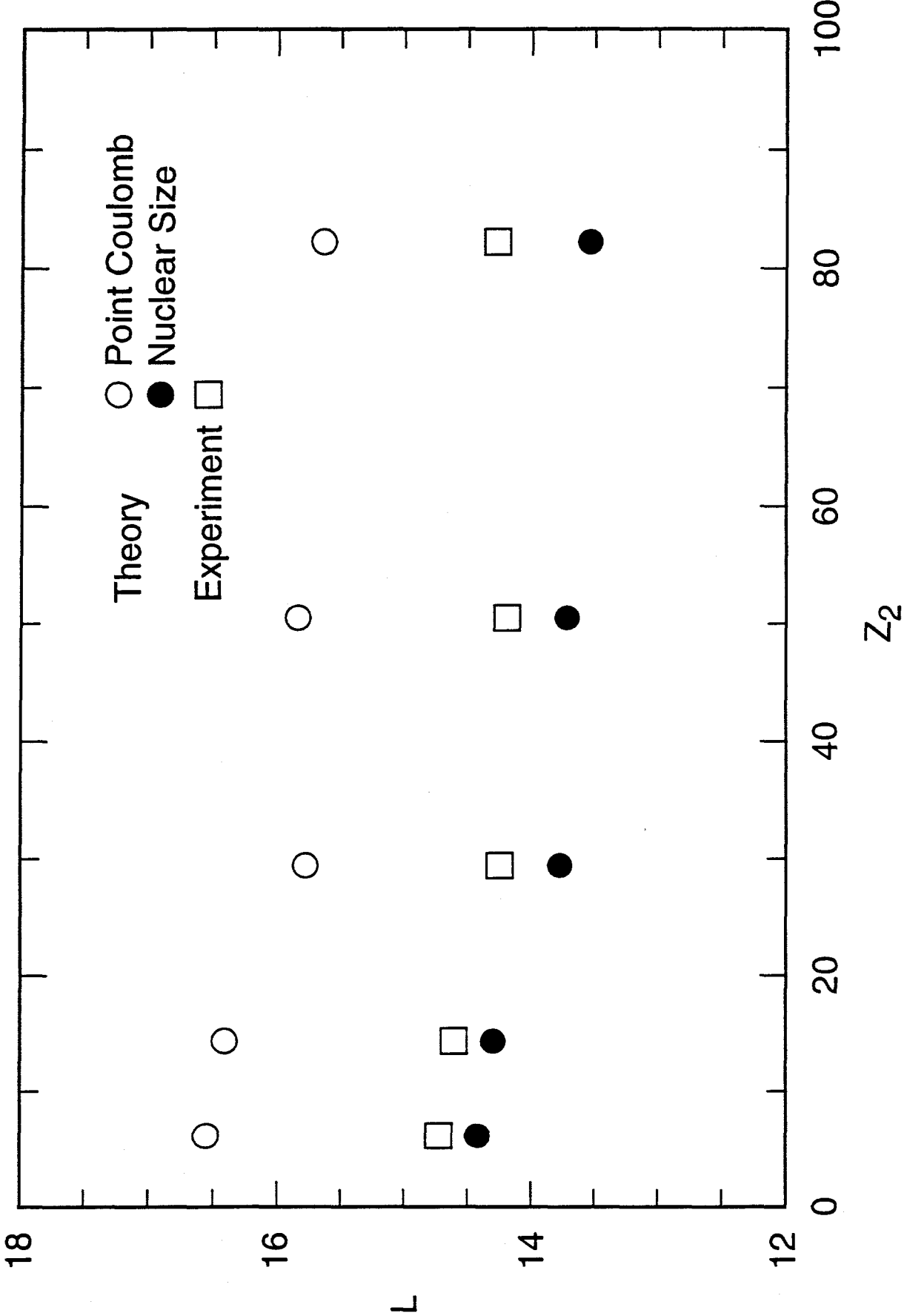


Figure 7

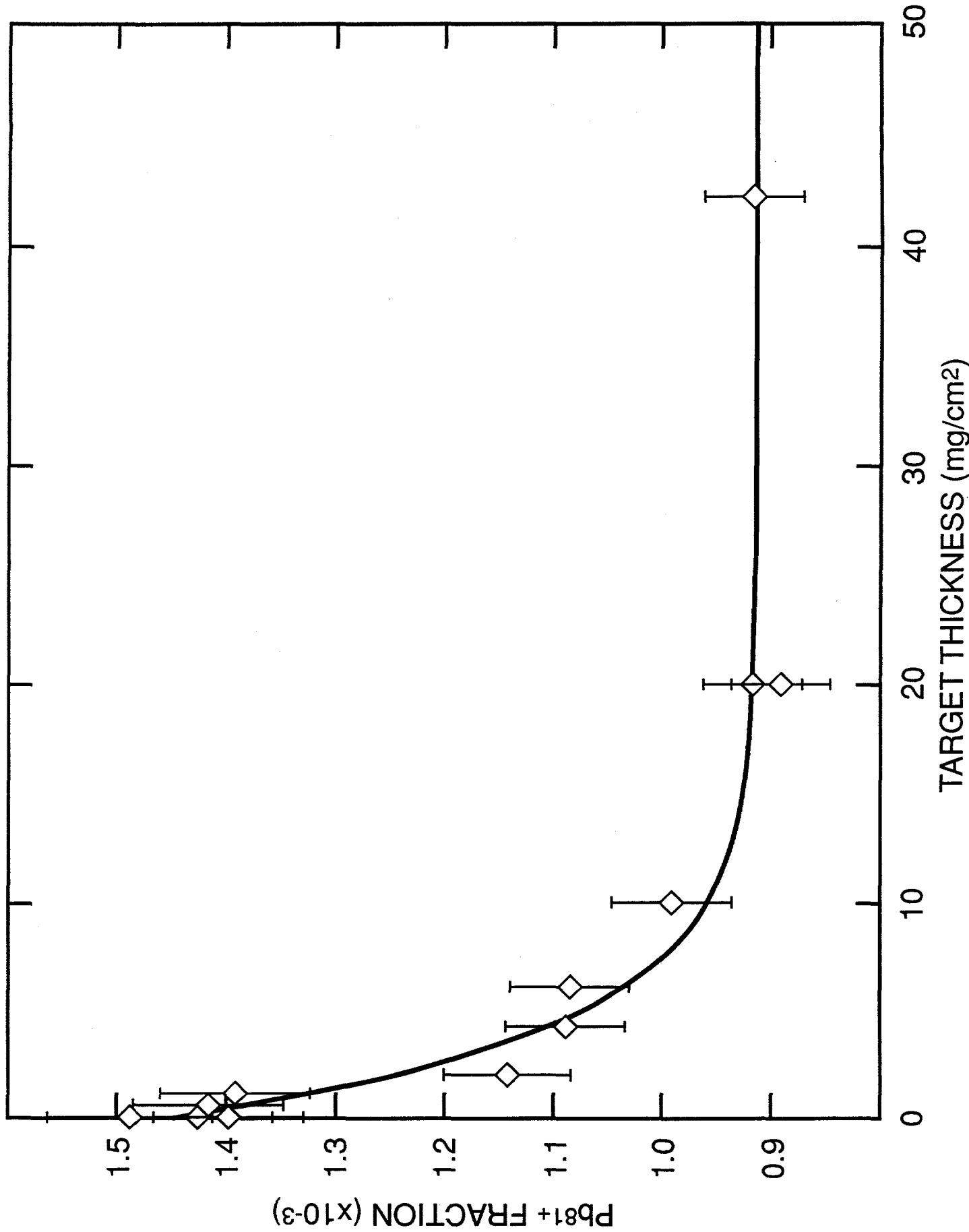


Figure 8

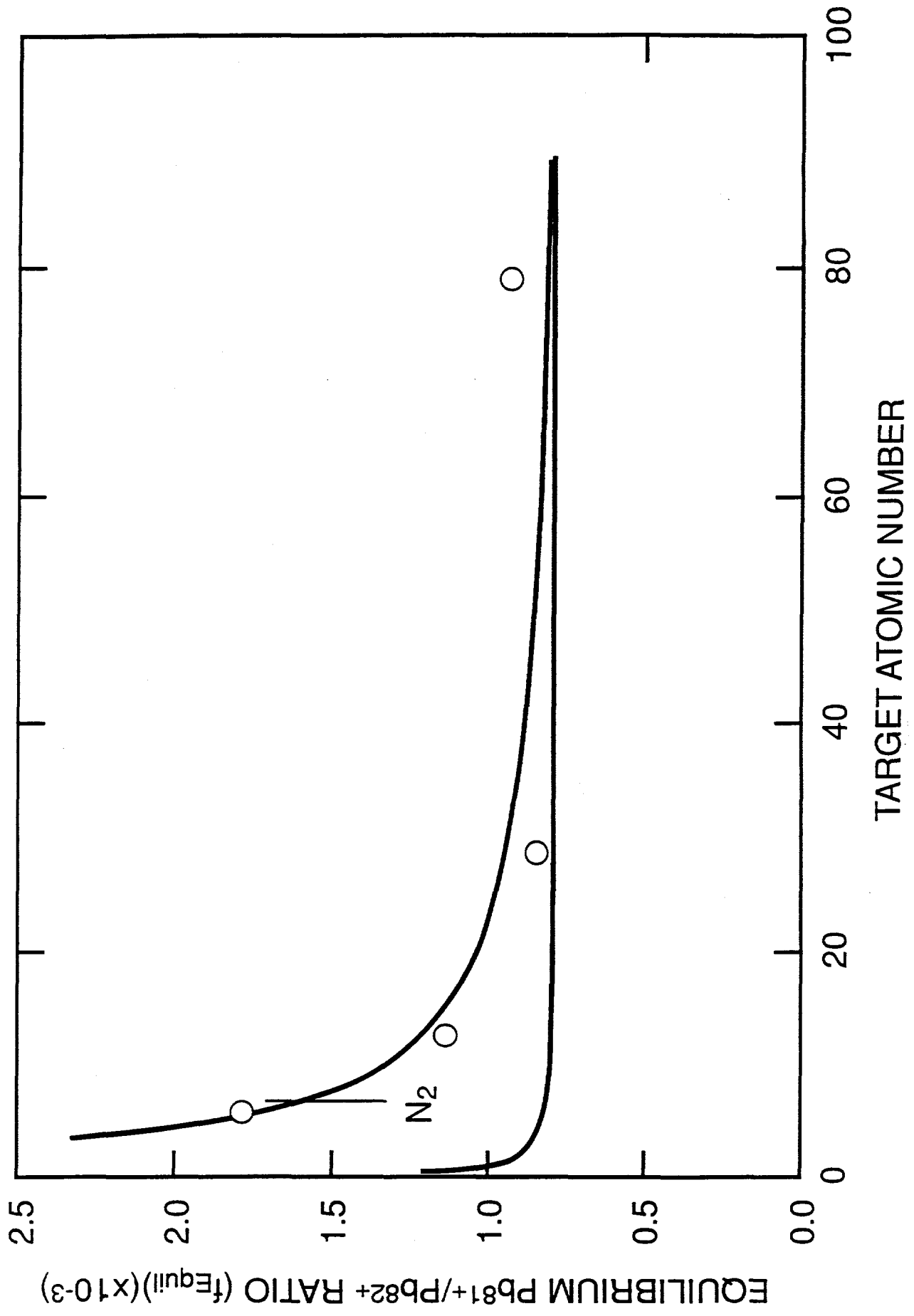


Figure 9